Title: Environmental disturbance in Agulhas rings affect inter-ocean plankton dispersal

E. Villar[1]*, S. Audic[2,3], L. Bittner[2,3,4 †], B. Blanke[5], J. R. Brum[6], C. Brunet[7], R. Casotti[7], A. Chase[8], J. R. Dolan[9,10], F. d'Ortenzio[9,10], G. Farrant[2,3], L. Garczarek[2,3], J.P. Gattuso[9,10], N. Grima[5], L. Guidi[9,10], C. N. Hill[11], O. Jahn[11], J. L. Jamet[12], H. Le Goff[13], C. Lepoivre[1], S. Malviya[4], E. Pelletier[14,15,16], J. B. Romagnan[9,10], S. Roux[6], S. Santini[1], E. Scalco[7], S.M. Schwenck[6], A. Tanaka[4‡], P. Testor[13], T. Vannier[14,15,16], F. Vincent[4], C. Dimier[2,3,4], M. Picheral[9,10], S. Searson[9,10††], S. Kandels-Lewis[17,18], *Tara* Oceans coordinators[§], S. G. Acinas[19], E. Boss[8], C. Bowler[4]*, C. de Vargas[2,3], M. Follows[11], G. Gorsky[9,10], H. Ogata[1‡‡], S. Pesant[20,21], S. Speich[5,22], M. B. Sullivan[6], S. Sunagawa[17], P. Wincker[14,15,16], A. Zingone[7], E. Karsenti[4,18]*, F. Not[2,3¶]*, P. Hingamp[1¶]*, D. Iudicone[7¶]*

Affiliations:

[1]Aix Marseille Université, CNRS, IGS UMR 7256, 13288, Marseille, France.
[2]CNRS, UMR 7144, Station Biologique de Roscoff, Place Georges Teissier, 29680 Roscoff, France.
[3]Sorbonne Universités, UPMC Univ Paris 06, UMR 7144, Station Biologique de Roscoff, Place Georges Teissier, 29680 Roscoff, France.
[4]Ecole Normale Supérieure, Institut de Biologie de l'ENS (IBENS), and Inserm U1024, and CNRS UMR 8197, Paris, F-75005 France.
[5]Laboratoire de Physique des Océans (LPO) UMR 6523 CNRS-Ifremer-IRD-UBO, Brest, France.
[6]Department of Ecology and Evolutionary Biology, University of Arizona, Tucson, AZ, 85721, USA.
[7]Zoologica Anton Dohrn, Villa Comunale, 80121, Naples, Italy.
[8]School of Marine Sciences, University of Maine, Orono, Maine, USA.
[9]Sorbonne Universités, UPMC Univ Paris 06, Observatoire Océanologique, F-06230 Villefranche-sur-mer, France.
[10]CNRS, UMR 7093, LOV, Observatoire Océanologique, F-06230 Villefranche-sur-mer, France.
[11]Department of Earth, Atmospheric and Planetary Sciences, Massachusetts Institute of Technology, Cambridge, USA.
[12]Université de Toulon, Laboratoire PROTEE-EBMA E.A. 3819, BP 20132, 83957 La Garde cedex, France.
[13]CNRS, UMR 7159, Laboratoire d'Oceanographie et du Climat LOCEAN, 4 place Jussieu, 75005, Paris, France.
[14]CEA - Institut de Génomique, GENOSCOPE, 2 rue Gaston Crémieux, 91057 Evry France.
[15]CNRS, UMR 8030, CP5706, Evry France.
[16]Université d'Evry, UMR 8030, CP5706, Evry France.
[17]Structural and Computational Biology, European Molecular Biology Laboratory, Meyerhofstr. 1, 69117 Heidelberg, Germany.
[18]Directors' Research European Molecular Biology Laboratory Meyerhofstr. 1, 69117 Heidelberg, Germany.
[19]Department of Marine Biology and Oceanography Institute of Marine Science (ICM)-CSIC Pg. Marítim de la Barceloneta 37-49 Barcelona E08003 Spain.
[20]PANGAEA, Data Publisher for Earth and Environmental Science, University of Bremen, Bremen, Germany.
[21]MARUM, Center for Marine Environmental Sciences, University of Bremen, Bremen, Germany.
[22]Department of Geosciences, Laboratoire de Météorologie Dynamique (LMD), Ecole Normale Supérieure, 24 rue Lhomond, 75231 Paris Cedex 05 France.

§ Tara Oceans coordinators and affiliations are listed on the companion web site.
† Current address: CNRS FR3631, Institut de Biologie Paris-Seine, F-75005, Paris, France / Sorbonne Universités, UPMC Univ Paris 06, Institut de Biologie Paris-Seine (IBPS), F-75005, Paris, France.
‡ Current address: Muroran Marine Station, Field science center for northern biosphere, Hokkaido university, Japan.
†† Current address: CMORE, University Hawaii, Honolulu, USA.
‡‡ Current address: Institute for Chemical Research, Kyoto University, Gokasho, Uji, Kyoto, 611-001, Japan.
¶ These authors contributed equally to this work.
*Correspondence to: villar@igs.cnrs-mrs.fr, not@sb-roscoff.fr, hingamp@igs.cnrs-mrs.fr, iudicone@szn.it, karsenti@embl.de, cbowler@biologie.ens.fr.

Abstract: Agulhas rings provide the principal route for ocean waters to circulate from the Indo-Pacific to the Atlantic basin. They strongly influence global ocean circulation but their influence on plankton transport is unknown. We show that while the coarse taxonomic structure of plankton communities is continuous across the Agulhas choke point, South Atlantic plankton diversity is altered compared to Indian Ocean source populations. Modelling and *in situ* sampling of a young Agulhas ring indicate that strong vertical mixing drives complex nitrogen cycling, shaping community metabolism and biogeochemical signatures as the ring and associated plankton transit westwards. The peculiar local environment inside Agulhas rings may provide a selective mechanism contributing to the limited dispersal of Indian Ocean plankton populations into the Atlantic.

One Sentence Summary: The distinct plankton diversity of South Atlantic versus Indian Ocean populations may be linked to the peculiar local environment of Agulhas rings.

Main Text:

Global ocean circulation is under the influence of Agulhas Current leakage, which connects the Indo-Pacific and Atlantic oceans (1). As a result of environmental forcing, the Agulhas leakage appear to be increasing over the last decades (2). Its strong influence on the oceanic conveyor belt makes this area of the world ocean a sensitive lever in climate change scenarios (3). Agulhas leakage has represented a compulsory gateway for planetary-scale water transport since the early Pleistocene (4), and diatom fossil records suggest that this choke point is not a barrier to plankton dispersal (5). Most of the leakage occurs through huge anticyclonic eddies, the Agulhas rings, 100-400 km in diameter, formed from Indian Ocean subtropical waters at the Agulhas Retroflection (1). Each year, up to half a dozen Agulhas rings escape the Indian Ocean, enter Cape Basin and drift north-westerly across the South Atlantic, reaching the South American continent over the course of several years (1,6). During their spawning in the “roaring forties”, extreme wind intensities induce severe environmental disturbances in Agulhas rings, such as intense cooling and substantial mixing (7). How the severe environmental changes occurring in Agulhas rings impact plankton inter-basin connectivity is a challenging question with potentially far reaching consequences, including effects on plankton diversity and species global distributions. Indeed, barriers to dispersal could undermine marine ecosystem resilience in the face of environmental change (8), as is the case for terrestrial ecosystems (9,10). Here we took advantage of the holistic sampling approach used during the *Tara* Oceans expedition (11) to produce a comprehensive description of the taxonomic and functional plankton assemblages inside Agulhas rings and across the three oceanic systems surrounding the Agulhas choke point: the western Indian Ocean (IO) subtropical gyre, the South Atlantic Ocean (SAO) gyre, and the Southern Ocean (SO), separated from the other two by the Antarctic Circumpolar Current (ACC) (Fig. 1).

Physical and biological oceanography of the Agulhas sampling sites

The IO, SAO and SO were each represented by three distinct sampling sites (sampled from May 2010 to January 2011, fig. 1 & table S1), covering a variety of environmental conditions across the three main oceanic systems (12, tables S2-S3). We sampled the two large contiguous IO and SAO subtropical gyres, and the Agulhas ring structures that maintain the physical connection between them. Specifically, on the western side of the IO station TARA_52 was characterized by

tropical, oligotrophic conditions. Station TARA_64 was located within an anticyclonic eddy representing the Agulhas Current recirculation. Station TARA_65 was located at the inner edge of the Agulhas Current on the South African slope that feeds the Agulhas retroflection and Agulhas ring formation (3). In the SAO, station TARA_70, a late winter station, was located in the eastern subtropical Atlantic basin. Station TARA_72 was located within the tropical circulation of the SAO, whilst station TARA_76 was at the north-west extreme of the SAO subtropical gyre. Two additional stations (TARA_68 & TARA_78) from the west and east SAO specifically sampled Agulhas rings. The last three stations were conducted in the SO to describe the ACC frontal system. Station TARA_82 sampled sub-Antarctic waters flowing northward along the Argentinian slope, waters whose fate is to flow along the ACC (13) with characteristics typical of summer sub-Antarctic surface waters, strongly stratified by seasonal heating. Station TARA_84 was located on the southern part of the ACC, in the Drake Passage and in between the Polar Front and the South ACC front (SACCF; 13). Finally, station TARA_85 was located on the southern edge of the SACCF with waters typical of polar regions.

We first compared overall plankton community structures between the three oceans using imaging and genetic surveys of samples from the epipelagic zone of each station (12, tables S4-S12). Prokaryotes, phyto- and zooplankton assemblages were similar across IO and SAO samples, whereas SO samples were outliers (Fig. 2A). Indeed, in IO and SAO, zooplankton communities were dominated by Calanoida, Cyclopoida (Oithonidae) and Poecilostomatoida copepods (12, table S5), whilst phytoplankton communities were mainly composed of chlorophytes, pelagophytes and haptophytes (12, table S6). In contrast, SO zooplankton communities were distinguished by a large contribution of *Limacina* spp. gastropods whereas Poecilostomatoida copepods were rare, and SO phytoplankton were dominated by diatoms and haptophytes. The south-north biological division was even more conspicuous with respect to prokaryotes, where cyanobacteria dominant in IO and SAO were absent in SO and were replaced by a high proportion of Flavobacteria and Rhodobacterales (12, table S11). In addition, virus concentrations in the <0.2 µm size fractions were significantly lower in the southernmost SO station (14), viral particles displayed significantly smaller capsid diameters in two of the three SO sampling sites (14) and two SO viromes had significantly lower richness compared to SAO and IO (45). Conversely, nucleocytoplasmic large DNA viruses did not show discriminating patterns (12, table S12). Nonetheless, two SO sampled sites contained measurable coccolithoviruses not observed in the two northern IO and SAO sea areas, with the notable exception of the TARA_68 Agulhas ring.

Biological connection across the Agulhas choke point

Beyond taxonomic annotations, the proportion of strictly identical V9 rDNA barcodes shared between samples (shared barcode richness, 15) demonstrated that despite a significantly smaller interface area, genetic material in common between IO and SAO was over three times larger than with SO (Fig. 2B, tables S13-S14 in 12). Indeed, whereas the IO-SAO inter-ocean shared barcodes richness (32±5%) was not significantly different from typical intra-ocean values (37±7%, Tukey post-hoc 0.95 confidence), inter-ocean shared barcode richness involving the SO were significantly lower (9±3%, Fig. 2C). This was confirmed by comparing the proportion of whole shotgun metagenomic reads shared between samples: both intra-oceanic and IO-SAO inter-ocean pairwise similarities were in the 18-30% range, whereas inter-ocean similarities with SO samples were only 5-6% (16). Thus, our observation that Indo-Atlantic inter-ocean genetic

similarity was statistically indistinguishable from intra-ocean genetic similarities on either side of the choke point revealed a high Indo-Atlantic biological connection despite the physical basin discontinuity. However, the data also showed that absolute barcode richness differed profoundly either side of the Agulhas choke point, with a strong effect of organism body size (Fig. 3A). In the prokaryote 0.2-3 µm size fraction, SAO barcode richness was significantly higher compared to the IO, whereas for eukaryotes larger than 20 µm in size the opposite trend was observed. We can not rule out the possibility that the higher prokaryote diversity observed in SAO might be at least partly due to a protocol artefact resulting from a difference in prefiltration pore size from 1.6 µm (IO) to 3 µm (SAO and SO). Overall, eukaryote diversity across the Agulhas system was higher in the smaller size fractions (as reported in the pan-oceanic *Tara* Oceans dataset, 17), and for all size fractions considered, samples from the SO were less diverse than samples from the SAO and IO (Fig. 3A).

When V9 rDNA barcodes were clustered by sequence similarity and considered at operational taxonomic unit (OTU) level (15), over half (57%) of the OTUs contained higher sub-OTU barcode richness in IO than in SAO, whereas less than a third (32%) of OTUs were richer in SAO, leaving only 11% as strictly cosmopolitan (Fig. 3B). Taken together, these 1307 OTUs represented 98% of the barcode abundance, indicating that the observed higher sub-OTU richness in the IO was not conferred by the rare biosphere. Certain taxa display notable sub-OTU richness biases across the choke point. Consistent with their relatively large size, Opisthokonta (mostly copepods), Rhizaria (such as radiolarians) and Stramenopiles (in particular diatoms) had much higher sub-OTU richness in the IO, whereas only small sized Hacrobia (mostly haptophytes) showed modest increased sub-OTU richness in the SAO. We hypothesize that the plankton filtering observed in fractions above 20 µm through the Agulhas choke point might also explain the diversity reduction observed for marine nekton from the IO to the south SAO (18), by propagating up the food-web as speculated by Cunha *et al.* (19).

In situ sampling of two Agulhas rings

To understand whether Agulhas rings, the main transporters of water across the choke point, might contribute to this IO to SAO diversity filtering, we analyzed data collected in both a young (YR) and an old ring (OR). The anticyclonic young ring sampled at station TARA_68 was located in Cape Basin west of South Africa, where rings are often observed after their formation at the Agulhas Retroflection (7,20). It was a large Agulhas ring that detached from the retroflection about 9-10 months prior to sampling. The newly formed Agulhas ring first moved northward and then westward in the Cape Basin while strongly interacting with other structures (red track in fig. 1b, 21). From satellite ocean color data interpolated on the ring trajectory, surface chlorophyll concentrations were higher in the Cape Basin than at the retroflection, suggesting that strong vertical mixing might have occurred in the Cape Basin (22). At the time of sampling, the anticyclonic structure had a diameter of 130-150 km, a sea surface height anomaly of about 30 cm and was surrounded by a small cyclonic eddy to the north and a larger one to the east (Fig. 4A, 23). The on-board thermosalinograph data showed that filaments of colder, fresher water surrounded the young ring core (Fig. 4A, 23). In order to position the biological sampling station close to the ring core, a series of CTD casts was performed (23, 24). The young Agulhas ring had a surface temperature and salinity of 16.8°C and 35.7 psu, respectively; the isopycnal sloping could be traced down to CTD maximal depth (900-1000m). Importantly, the core of the ring water was 5°C cooler than IO subtropical source waters at similar latitudes (TARA_65, table

S1) and was very similar to typical values for the IO subtropical waters south of Africa (17.8°C, 35.56 psu, respectively, according to 25). The young Agulhas ring had a particularly deep mixed layer (>250m) compared to climatological seasonal cycles of the mixed layer depths in the region (50-100m, fig. 4C), consistent with previous ring observations (26). At larger scales (Fig. 4B, 24), steep spatial gradients were observed, with fresher and colder water in the Cape Basin than in the Agulhas Current because of both lateral mixing with waters from the South and surface fluxes. This confirms that the low temperature of the young Agulhas ring is a general feature of this IO to SAO transitional basin. Air-sea exchanges of heat and momentum promoted an intense convection in the ring core, which was not compensated by lateral mixing and advection. These data therefore suggest that the core of the Agulhas ring behaved as a sub-polar environment traveling across sub-tropical regions. At station TARA_78 we sampled a second structure whose origins were in the Agulhas Retroflection, likely a 3-year-old Agulhas ring. This old ring, having crossed the SAO, was being absorbed by the western boundary current of the SAO subtropical gyre.

Biologically, the overall plankton assemblage of both Agulhas rings most closely resembled the cluster of IO and SAO stations (Fig. 2A). This trend was confirmed when considering shared V9 rDNA barcode richness between samples: Agulhas rings were similar to IO and SAO in proportions comparable to intra-ocean similarities (Fig. 2B & 2C). However, a modest but significant (Tukey post-hoc .95 confidence) increase in ring shared barcode richness with their surrounding SAO samples versus their IO origins was observed (Fig. 2C). In whole shotgun metagenomic read comparisons (16), the old ring appeared as a typical SAO sample whereas the young ring stood out as distinct from both IA and SAO. This was supported by light microscopy analyses which revealed some plankton groups specific to the young Agulhas ring, such as *Pseudo-nitzschia* spp. which represented 20% of the phytoplankton counts observed in the young ring, whilst being mostly undetected by microscopy in all other stations (12, table S8). Other potentially circumstantial plankton characteristic of the young Agulhas ring included the tintinnid *Dictyocysta pacifica* (12, table S7), the diatom *Corethron pennatum* (12, table S8), and the dinoflagellate *Tripos limulus* (12, table S9). Interestingly, a tiny pennate diatom from the genus *Nanoneis* was exclusively observed in the young Agulhas ring and IO stations around the African coasts (27). The latter species was an example observed by microscopy of the Indo-Atlantic plankton diversity filtering observed at V9 rDNA barcode level. OTU clustered barcodes revealed a variety of sub-OTU richness patterns around the young Agulhas ring (Fig. 5A). Amongst Copepoda, *Gaetanus variabilis* and *Corycaeus speciosus* were the more cosmopolitan species (Fig. 5B), whilst *Bradya* species found in the ring were mainly similar to those from the IO. *Acartia negligens* and *Neocalanus robustior* displayed high levels of sub-OTU barcode richness specific to each side of the Agulhas choke point. Bacillariophyceae were heavily filtered from IO to SAO (Fig. 5C), and most OTUs (17 out of 20) were absent in the young ring, suggesting diversity filtering could take place earlier in the ring's nine months history. Consistent with the observed particularities of the plankton in the young ring, continuous underway optical measurements showed that the ring core photosynthetic community differed significantly from surrounding waters (28). Intermediate size cells, and relatively low content of photo-protective pigments, reflected low growth irradiance and suggested a transitional physiological state. Thus, the plankton community in the young Agulhas ring had clearly diverged from its original IO waters, but nine months after formation it had not yet converged with its surrounding SAO waters.

Deep mixing in Agulhas rings promotes plankton bloom

An unexpected characteristic in the upper water column of the young ring was an unusually high nitrite concentration (>0.5 mmol.m-3) (Fig. 4D, 29). This observation, along with its particularly deep mixed layer (>250m), suggested that as Agulhas rings proceed westward in the Cape Basin, vigorous deep mixing of their weakly stratified waters may have entrained nitrate and stimulated phytoplankton blooms. Typically, fresh organic material would then either be exported as sinking particles or locally recycled, sustaining heterotrophic production of ammonium which would, in turn, be consumed by photoautotrophs in the euphotic layer but nitrified below. The resulting nitrite, eventually oxidized to nitrate, might remain evident at subsurface as observed in the nitrite anomaly of the young ring explored here. This hypothesis was supported by numerical simulations with a high physical and biological resolution configuration of the MITgcm ocean model (30) which resolved Agulhas rings, their phytoplankton populations and associated nutrient cycling (Fig. 6A). We tracked 12 Agulhas rings in the ocean model and characterized their (near) surface biogeochemical cycles (Fig. 6B, 31). Consistently, as the weakly stratified rings moved westwards, storms enhanced surface heat loss stimulating convection and the entrainment of nitrate. As hypothesized above, in the model simulations the virtual proliferation of phytoplankton resulted in a subsurface slug of nitrite, which persisted because phytoplankton were light limited at depth and because nitrification was suppressed by light at the surface (32). The associated blooms were dominated by large opportunistic phytoplankton and nitrate-metabolizing *Synechococcus* spp. analogs, whereas populations of *Prochlorococcus* spp. analogs dominated the quiescent periods (31). Each of the 12 simulated Agulhas rings exhibited this pattern in response to surface forcing by weather systems, and all rings maintained a persistent subsurface nitrite maximum in the region, as observed in TARA_68 and in other biogeochemical surveys (33).

The nitrite peak observed in the TARA_68 young Agulhas ring was associated with a differential representation of nitrogen metabolism genes between the ring and the surrounding SAO and IO metagenomes derived from the 0.2-3 µm size fraction (Fig. 7, table S15 in 12). Agulhas ring over-represented KEGG orthologs (KOs) were involved in both nitrification and denitrification, likely representing the overlap between plankton assemblages involved in the conversion of nitrate to nitrite on the one hand, and in denitrification of the accumulating nitrite on the other. This was supported by the observation that distinct KOs involved in successive denitrification steps were found to be encoded by similar plankton taxa. For instance K10945 and K10946 involved in ammonium nitrification and K00368 subsequently involved in nitrite to nitrous oxide denitrification appeared mostly encoded by Nitrosopumilaceae archaea. K00264 and K01674 involved in ammonium assimilation were mostly assigned to eukaryotic Mamiellales, whilst the opposite K00367 and K00366 involved in dissimilatory nitrite reduction to ammonium followed by K01725 involved in ammonium assimilation were encoded by picocyanobacteria.

In the specific case of the picocyanobacteria, metagenomic reads corresponding to *nirA* genes showed that the observed young Agulhas ring KO00366 (dissimilatory nitrite reduction) enrichment was mainly due to the over-representation of genes from *Prochlorococcus* (Fig. 8B). This enrichment was found to be associated with a concomitant shift in population structure from *Prochlorococcus* High Light II ecotypes (HLII mostly lacking *nirA* genes) to co-dominance of High Light I (HLI) and Low Light I (LLI) ecotypes. Indeed, among the several *Prochlorococcus* and *Synechococcus* ecotypes identified based on their genetic diversity and physiology (34,35),

neutral marker (*petB*, fig. 8A) recruitments showed that dominant clades in the IO upper mixed layer were *Prochlorococcus* HLII and *Synechococcus* clade II, as expected given the known (sub)tropical preferenda of these groups (36). Both clades nearly completely disappeared in the mixed cold waters of the young ring and only began to increase again when the surface water warmed up along the SAO transect. Conversely, young ring water was characterized by a large proportion of *Prochlorococcus* HLI and LLI and *Synechococcus* clade IV, two clades typical of temperate waters. Besides temperature, the *Prochlorococcus* community shift from HLII to HLI + LLI observed in the young ring was likely also driven by the nitrite anomaly. Indeed, while most *Synechococcus* strains isolated so far are able to use nitrate, nitrite and ammonium, only the *Prochlorococcus* LLI and IV and some populations of HL clades, having acquired the *nirA* gene by lateral gene transfer, are able to assimilate nitrite. In the young ring, over-representation of cyanobacterial orthologs involved in nitrite reduction could thus have resulted from environmental pressure selecting LLI (87% of the nirA recruitments) and HLI populations (13%) that possessed this ability. Since the capacity to assimilate nitrite in this latter ecotype has been shown to reflect the availability of this nutrient in the environment (37), these *in situ* observations of picocyanobacteria indicated that the nitrogen cycle disturbance occurring in the young ring was powerful enough to exert community wide selective pressure on Agulhas ring plankton.

Discussion

We found that whether or not the Agulhas choke point is considered a barrier to plankton dispersal depends on the taxonomic resolution at which the analysis is performed. At coarse taxonomic resolution, our observations of Indo-Atlantic continuous plankton structure - from viruses to fish larvae - were consistent with unlimited dispersal hypotheses (5, 38). However, as anticipated in (5), at finer sub-OTU resolution our data revealed that the Agulhas choke point was a barrier strongly affecting patterns of plankton diversity. Thus, rather than a panmictic ocean, our data suggest the existence of dispersal filters, consistent with anecdotal single species reports (39, 40). The lower diversity observed here in SAO for micro- and mesoplankton (>20 µm) may be due to local abiotic/biotic pressure, and/or to limitations in dispersal (30, 41). In any case, such plankton diversity patterns indicate that the SAO is distinct despite being downstream of the Indo-Pacific basin. It is also intriguing that the biogeography emerging from a model with only neutral drift (42) predicts basin-to-basin genetic differences that are qualitatively consistent with our data. The issue of the relative role of selection and neutral drift in the observed patterns remains open, although the observed acquisition of *nirA* genes by HLI *Prochlorococcus* in the young Agulhas ring suggests the former might be at work in Agulhas rings. Considering the breadth of the changes observed in the 9-month-old Agulhas ring, it would be interesting to acquire samples from specific Agulhas rings tracked from formation to dissipation.

Based on our *in situ* integrative analysis of two Agulhas rings, we propose that ring environmental disturbances significantly reshape local plankton diversity during transit between IO and SAO. This disturbance might represent the marine equivalent of the metabolic barriers which are well established and intensively studied in terrestrial systems (9,10). Furthermore, we show that taxonomic groups were not equally affected by the ring transport, both within and between phyla, with a noticeable effect of organism size. With increasing awareness of the breadth of ocean plankton diversity (17), these heterogeneous responses to environmental changes highlight the difficulty in generalizing ecological/evolutionary rules from few reference species or functional types. Emerging models should take into account how environmental

selection applied at key ocean circulation choke points *de facto* constitute dispersal barriers. Considering sensitivity of Agulhas leakage to climate change (1, 43), better understanding of the plankton dynamics in these distinct ring environments will be required if we are to understand, and even predict, plankton resilience at the planetary scale. Finally, our data suggest that the abundance of IO species in SAO sedimentary records, used as proxies of Agulhas Leakage intensity (4), may actually also depend on the intensity of the Agulhas ring physical disturbances.

Materials & Methods

Sampling

The Tara Oceans sampling protocols schematized in Karsenti *et al.* (11) are described in Pesant *et al.* (44), specific methods for 0.8-5, 20-180 & 180-2000 µm size fractions in de Vargas *et al.* (17), for 0.2-3 µm size fractions in Sunagawa *et al.* (45), and for the <0.2 µm size fraction in Brum *et al.* (46). Due to their fragility, 1.6 µm glass fiber filters initially used for prokaryote sampling were replaced by more resistant 3 µm polycarbonate filters from station TARA_66 onwards. In the present text, both 0.2-1.6 µm and 0.2-3 µm prokaryote size fractions are simply referred to as 0.2-3 µm.

Data acquisition

A range of analytical methods covering different levels of taxonomic resolution (pigments, flow cytometry, optical microscopy, marker gene barcodes, metagenomics) were used to describe the planktonic composition at each sampled station. Viruses from the <0.2 µm size fraction were studied both by epifluorescence microscopy, quantitative transmission electron microscopy and by sequencing DNA as described in Brum *et al.* (46). Flow cytometry was used to discriminate high DNA content bacteria (HNA), low DNA content bacteria (LNA), *Prochlorococcus* and *Synechococcus* picocyanobacteria, as well as two different groups (based on their size) of photosynthetic picoeukaryotes as described previously (47). Pigment concentrations measured by High Performance Liquid Chromatography (HPLC) were used to estimate the dominant classes of phytoplankton using the CHEMTAX procedure (48). Tintinnids, diatoms and dinoflagellates were identified and counted by light microscopy from the 20-180 µm lugol or formaldehyde fixed size fraction. Zooplankton enumeration was performed on formol fixed samples using the ZOOSCAN semi-automated classification of digital images (49). Sequencing, clustering and annotation of 18S-V9 rDNA barcodes are described in de Vargas *et al.* (17). Metagenome sequencing, assembly and annotation are described in Sunagawa *et al.* (45). NCLDV taxonomic assignations in the 0.2-3 µm samples were carried out using 18 lineage specific markers as described in Hingamp *et al*. (50). Virome sequencing and annotation are described in Brum *et al.* (46).

Tara Oceans environmental data and sampling metadata are available at PANGAEA under project label “TOC” (http://www.pangaea.de/?q=project:label:TOC). The list of PANGAEA sample accession numbers specifically used in the present Agulhas system study are provided in table S1. The Tara Oceans nucleotide sequences (17, 45, 46) are available at the European Nucleotide Archive (ENA) under project ID PRJEB402 (http://www.ebi.ac.uk/ena/data/view/PRJEB402).

Data analysis

Origin of sampled Agulhas rings

Using visual and automated approaches, the origins of the TARA_68 and TARA_78 stations was traced back from the altimetric daily data (Fig. 1, 21). The automated approach used either the Lagrangian tracing of numerical particles initialized in the centre of a given structure and transported by the geostrophic velocity field calculated from sea surface height gradients, or the connection in space and time of adjacent extreme values in sea level anomaly maps.

V9 rDNA barcodes

To normalize for differences in sequencing effort, V9 rDNA barcode libraries were resampled 50 times for the number of reads corresponding to the smallest library in each size fraction: 0.8-5 µm: 776,358 reads, 20-180 µm: 1,170,592 reads and 180-2000 µm: 767,940 reads. V9 rDNA barcode counts were then converted to the average number of times seen in the 50 resampling events and barcodes with less than 10 reads were removed as potential sequencing artefacts. We used down-sampled barcode richness (number of distinct V9 rDNA barcodes) as a diversity descriptor since considering V9 rDNA barcode abundances to compare plankton assemblages would likely be biased due: i/ to technical limitations described in de Vargas *et al.* (17), and ii/ to seasonality effects induced by the timing of samplings (Table S1). Barcode richness was well correlated with Shannon and Simpson indexes (0.94 and 0.78, respectively). The shared barcode richness between each pair of samples (15) was estimated by counting for the three larger size fractions (0.8-5, 20-180 & 180-2000 µm) the proportion of V9 rDNA barcodes 100% identical over their whole length. V9 rDNA barcodes were clustered into OTUs by SWARM clustering as described by de Vargas *et al.* (17). The sub-OTU richness comparison between two samples s1 and s2 (15) produces three values: the number of V9 rDNA barcodes in common, the number of V9 rDNA barcodes unique to s1, and the number of V9 rDNA barcodes unique to s2. These numbers can be represented directly as bar graphs (Fig. 3B) or as dot plots of specific V9 rDNA barcode richness (Fig. 5).

Metagenomic analysis

Similarity was estimated using whole shotgun metagenomes for all four available size fractions (0.2-3, 0.8-5, 20-180 & 180-2 000 µm). Because pairwise comparisons of all raw metagenome reads is intractable given the present data volume, we used a heuristic where two metagenomic 100 bp reads were considered similar if at least two non overlapping 33 bp kmers were strictly identical (Compareads method, 51). For prokaryotic fractions (0.2-3 µm), taxonomic abundance was estimated using the number of 16S miTags (45). The functional annotation, taxonomic assignation and gene abundance estimation of the pan oceanic Ocean Microbial Reference Gene Catalog (OMRGC, 243 samples including all those analysed here) generated from *Tara* Oceans 0.2-3 µm metagenomic reads are described in Sunagawa *et al.* (45). Gene abundances were computed for the set of genes annotated to nitrogen metabolism KEGG ortholog (KO, 52) group by counting the number of reads from each sample that mapped to each KO associated gene. Abundances were normalized as Reads Per Kilobase per Million mapped reads (RPKM). Gene abundances were then aggregated (summed) for each KO group. To compare abundances between the young ring (TARA_68) and other stations, a t-test was used. KOs with a p-value < 0.05 and a total abundance (over all stations) > 10 were considered as significant (12, table S15).

Prochlorococcus and *Synechococcus* community composition was analyzed in the 0.2-3 µm size fraction at the clade level by recruiting reads targeting the high resolution marker gene *petB*,

coding for cytochrome b_6 (53). The *petB* reads were first extracted from metagenomes using BLASTx+ against the *petB* sequences of *Synechococcus* sp. WH8102 and *Prochlorococcus marinus* MED4. These reads were subsequently aligned against a reference dataset of 270 *petB* sequences using BLASTn (with parameters set at -G 8 -E 6 -r 5 -q -4 -W 8 -e 1 -F "m L" -U T). *petB* reads exhibiting > 80% identity over > 90% of sequence length were then taxonomically assigned to the clade of the best BLAST hit. Read counts per clade were normalized based on the sequencing effort for each metagenomic sample. A similar approach was used with *nirA* (KO 00366) and *narB* genes (KO 00367) which were highlighted in the nitrogen-related KO analysis (Fig. 8). Phylogenetic assignment was realized at the highest possible taxonomic level using a reference dataset constituted of sequences retrieved from Cyanorak v2 (www.sb-roscoff.fr/cyanorak/) and GOS (54, 37) databases.

Nitrogen cycle modelling

Numerical simulations of global ocean circulation were based on the Massachusetts Institute of Technology general circulation model (MITgcm; 55) incorporating biogeochemical and ecological components (56, 57). It resolved mesoscale features in the tropics and was eddy permitting in sub-polar regions. The physical configurations were integrated from 1992 to 1999 and constrained to be consistent with observed hydrography and altimetry (58). Three inorganic fixed nitrogen pools were resolved: nitrate, nitrite and ammonium, as well as particulate and dissolved detrital organic nitrogen. Phytoplankton types were able to use some or all of the fixed nitrogen pools. Aerobic respiration and remineralization by heterotrophic microbes was parameterized as a simple sequence of transformations from detrital organic nitrogen, to ammonium, then nitrification to nitrite and nitrate. In accordance with empirical evidence (32), nitrification was assumed to be inhibited by light. Nitrification is described in the model by simple first order kinetics, with rates tuned to qualitatively capture the patterns of nitrogen species in the Atlantic (57).

Continuous spectral analysis

A continuous flow-through system equipped with a high-spectral-resolution spectrophotometer (AC-S, WET Labs, Inc.) was used for data collection during the *Tara* Oceans expedition as described previously (59). Phytoplankton pigment concentrations, estimates of phytoplankton size γ, total chlorophyll a concentration, and particulate organic carbon (POC) are derived from the absorption and attenuation spectra (60) for the 1-km2-binned Tara Oceans data set available at PANGAEA under project label “Tara Oceans” (http://www.pangaea.de).

References and Notes:

1. Biastoch, C. W. Böning, J. R. E. Lutjeharms, Agulhas leakage dynamics affects decadal variability in Atlantic overturning circulation, Nature 456, 489–492 (2008).
2. Biastoch, C. W. Böning, F. U. Schwarzkopf, J. R. E. Lutjeharms, Increase in Agulhas leakage due to poleward shift of Southern Hemisphere westerlies, Nature 462, 495–498 (2009).
3. L. M. Beal, W. P. M. D. Ruijter, A. Biastoch, R. Zahn, S. W. G. 136, On the role of the Agulhas system in ocean circulation and climate, Nature 472, 429–436 (2011).
4. F. J. C. Peeters *et al.*, Vigorous exchange between the Indian and Atlantic oceans at the end of the past five glacial periods, Nature 430, 661–665 (2004).
5. P. Cermeño, P. G. Falkowski, Controls on Diatom Biogeography in the Ocean, Science 325, 1539–1541 (2009).

6. A. L. Gordon, Oceanography: The brawniest retroflection. Nature. 421, 904–905 (2003).
7. H. M. van Aken *et al.*, Observations of a young Agulhas ring, Astrid, during MARE in March 2000. Deep Sea Research Part II: Topical Studies in Oceanography. 50, 167–195 (2003).
8. J. R. Bernhardt, H. M. Leslie, Resilience to Climate Change in Coastal Marine Ecosystems. Annual Review of Marine Science, 5: 371-392 (2013).
9. D. H. Janzen, Why mountain passes are higher in the tropics. American Naturalist 233-249 (1967).
10. G. Wang, M. E. Dillon, Recent geographic convergence in diurnal and annual temperature cycling flattens global thermal profiles. Nature Climate Change 4, 988–992, (2014).
11. E. Karsenti *et al.*, A Holistic Approach to Marine Eco-Systems Biology, PLoS Biol 9, e1001177 (2011).
12. Supplementary tables S1-S16 available at http://annotathon.org/Tara_Agulhas/#TableS
13. A.H. Orsi, T. Whitworth III, W. D. Nowlin Jr., On the meridional extent and fronts of the Antarctic Circumpolar Current. Deep-Sea Res. Part 1 42, 641–673 (1995)
14. Supplementary figure S1 available at http://annotathon.org/Tara_Agulhas/#FigS1
15. Supplementary figure S2 available at http://annotathon.org/Tara_Agulhas/#FigS2
16. Supplementary figure S3 available at http://annotathon.org/Tara_Agulhas/#FigS3
17. de Vargas *et al*., Sea change in eukaryotic plankton diversity, submitted.
18. W. Bowen, L. A. Rocha, R. J. Toonen, S. A. Karl, The origins of tropical marine biodiversity, Trends in Ecology & Evolution 28, 359–366 (2013).
19. R. L. Cunha *et al*., Ancient Divergence in the Trans-Oceanic Deep-Sea Shark Centroscymnus crepidater. PLoS ONE. 7, e49196 (2012).
20. Schmid *et al*., Early evolution of an Agulhas Ring. Deep Sea Research Part II: Topical Studies in Oceanography. 50, 141–166 (2003).
21. Supplementary figure S4 available at http://annotathon.org/Tara_Agulhas/#FigS4
22. Supplementary figure S5 available at http://annotathon.org/Tara_Agulhas/#FigS5
23. Supplementary figure S6 available at http://annotathon.org/Tara_Agulhas/#FigS6
24. Supplementary figure S7 available at http://annotathon.org/Tara_Agulhas/#FigS7
25. L. Gordon, J. R. Lutjeharms, M. L. Gründlingh, Stratification and circulation at the Agulhas Retroflection. Deep Sea Research Part A. Oceanographic Research Papers. 34, 565–599 (1987).
26. V. Faure, M. Arhan, S. Speich, S. Gladyshev, Heat budget of the surface mixed layer south of Africa. Ocean Dynamics. 61, 1441–1458 (2011).
27. Supplementary figure S8 available at http://annotathon.org/Tara_Agulhas/#FigS8
28. Supplementary figure S9 available at http://annotathon.org/Tara_Agulhas/#FigS9
29. Supplementary figure S11 available at http://annotathon.org/Tara_Agulhas/#FigS11
30. S. Clayton, S. Dutkiewicz, O. Jahn, M. J. Follows, Dispersal, eddies, and the diversity of marine phytoplankton, Limnology & Oceanography: Fluids & Environments 3, 182–197 (2013).
31. Supplementary figure S12 available at http://annotathon.org/Tara_Agulhas/#FigS12
32. R. J. Olson, Differential photoinhibition of marine nitrifying bacteria: a possible mechanism for the formation of the primary nitrite maximum. J. mar. Res. 39, 227–238 (1981).
33. S. Levitus *et al.*, The World Ocean Database. Data Science Journal. 12, WDS229–WDS234 (2013).
34. D. J. Scanlan *et al.*, Ecological genomics of marine picocyanobacteria. Microbiology and Molecular Biology Reviews. 73, 249–299 (2009).
35. Z. I. Johnson *et al.*, Niche Partitioning Among *Prochlorococcus* Ecotypes Along Ocean-Scale Environmental Gradients. Science. 311, 1737–1740 (2006).

36. K. Zwirglmaier *et al.*, Global phylogeography of marine *Synechococcus* and *Prochlorococcus* reveals a distinct partitioning of lineages among oceanic biomes. Environmental microbiology. 10, 147–161 (2008).
37. A. C. Martiny, S. Kathuria, P. M. Berube, Widespread metabolic potential for nitrite and nitrate assimilation among *Prochlorococcus* ecotypes. PNAS. 106, 10787–10792 (2009).
38. Hubert *et al*., A Constant Flux of Diverse Thermophilic Bacteria into the Cold Arctic Seabed. Science. 325, 1541–1544 (2009).
39. K. C. Churchill, Á. Valdés, D. Ó. Foighil, Afro-Eurasia and the Americas present barriers to gene flow for the cosmopolitan neustonic nudibranch *Glaucus atlanticus*. Mar Biol. 161, 899–910 (2014).
40. N. Selje, M. Simon, T. Brinkhoff, A newly discovered Roseobacter cluster in temperate and polar oceans. Nature. 427, 445–448 (2004).
41. Casteleyn *et al.*, Limits to gene flow in a cosmopolitan marine planktonic diatom. PNAS. 107, 12952–12957 (2010).
42. L. Hellweger, E. van Sebille, N. D. Fredrick, Biogeographic patterns in ocean microbes emerge in a neutral agent-based model. Science. 345, 1346–1349 (2014).
43. C. Backeberg, P. Penven, M. Rouault, Impact of intensified Indian Ocean winds on mesoscale variability in the Agulhas system, Nature Clim. Change 2, 608–612 (2012).
44. S. Pesant *et al.*, Tara Oceans Data: A sampling strategy and methodology for the study of marine plankton in their environmental context, submitted.
45. S. Sunagawa *et al*., Structure and function of the global ocean microbiome, submitted.
46. J. R. Brum *et al.*, Global patterns and ecological drivers of ocean viral communities, submitted.
47. J. M. Gasol, P. A. Del Giorgio, Using flow cytometry for counting natural planktonic bacteria and understanding the structure of planktonic bacterial communities; Scientia Marina. 64 (2000).
48. M. Mackey, D. Mackey, H. Higgins, S. Wright, CHEMTAX - a program for estimating class abundances from chemical markers: application to HPLC measurements of phytoplankton. Mar. Ecol. Progr. Ser. 144, 265–283 (1996).
49. G. Gorsky *et al.*, Digital zooplankton image analysis using the ZooScan integrated system. J. Plankton Res. 32, 285–303 (2010).
50. P. Hingamp *et al.*, Exploring nucleo-cytoplasmic large DNA viruses in *Tara* Oceans microbial metagenomes. ISME J. 7, 1678–1695 (2013).
51. N. Maillet, C. Lemaitre, R. Chikhi, D. Lavenier, P. Peterlongo, Compareads: comparing huge metagenomic experiments. BMC Bioinformatics. 13, S10 (2012).
52. M. Kanehisa *et al.*, KEGG for linking genomes to life and the environment. Nucleic Acids Research. 36, D480 (2008).
53. S. Mazard, M. Ostrowski, F. Partensky, D. J. Scanlan, Multi-locus sequence analysis, taxonomic resolution and biogeography of marine *Synechococcus*. Environmental Microbiology. 14, 372–386 (2012).
54. B. Rusch *et al.*, The Sorcerer II Global Ocean Sampling Expedition: Northwest Atlantic through Eastern Tropical Pacific. PLoS Biol. 5, e77 (2007).
55. J. Marshall, A. Adcroft, C. Hill, L. Perelman, C. Heisey, A finite-volume, incompressible Navier Stokes model for studies of the ocean on parallel computers. J. Geophys. Res.-Oceans. 102, 5753–5766 (1997).

56. M. J. Follows, S. Dutkiewicz, S. Grant, S. W. Chisholm, Emergent Biogeography of Microbial Communities in a Model Ocean. Science. 315, 1843–1846 (2007).
57. S. Dutkiewicz, M. J. Follows, J. G. Bragg, Modeling the coupling of ocean ecology and biogeochemistry. Global Biogeochem. Cycles. 23, GB4017 (2009).
58. Menemenlis *et al*., ECCO2: High resolution global ocean and sea ice data synthesis. Mercator Ocean Quarterly Newsletter. 31, 13–21 (2008).
59. A. Chase *et al.*, Decomposition of in situ particulate absorption spectra. Methods in Oceanography. 7, 110–124 (2013).
60. E. Boss *et al.*, The characteristics of particulate absorption, scattering and attenuation coefficients in the surface ocean; Contribution of the Tara Oceans expedition. Methods in Oceanography. 7, 52–62 (2013).
61. K.R. Ridgway , J.R. Dunn, and J.L. Wilkin, Ocean interpolation by four-dimensional least squares - Application to the waters around Australia, J. Atmos. Ocean. Tech., 19, No 9, 1357-1375 (2002)

Acknowledgments:

We thank the commitment of the following people and sponsors: CNRS (in particular Groupement de Recherche GDR3280), European Molecular Biology Laboratory (EMBL), Genoscope/CEA, VIB, Stazione Zoologica Anton Dohrn, UNIMIB, Fund for Scientific Research – Flanders, Rega Institute, KU Leuven, The French Ministry of Research, the French Government 'Investissements d'Avenir' programmes OCEANOMICS (ANR-11-BTBR-0008), FRANCE GENOMIQUE (ANR-10-INBS-09-08), MEMO LIFE (ANR-10-LABX-54), PSL* Research University (ANR-11-IDEX-0001-02), ANR (projects POSEIDON/ANR-09-BLAN-0348, PHYTBACK/ANR-2010-1709-01, PROMETHEUS/ANR-09-PCS-GENM-217, TARA-GIRUS/ANR-09-PCS-GENM-218), European Union FP7 (MicroB3/No.287589, IHMS/HEALTH-F4-2010-261376), ERC Advanced Grant Award to CB (Diatomite: 294823), Gordon and Betty Moore Foundation grant (#3790) to MBS, Spanish Ministry of Science and Innovation grant CGL2011-26848/BOS MicroOcean PANGENOMICS to SGA, TANIT (CONES 2010-0036) from the Agència de Gestió d´Ajusts Universitaris i Reserca to SGA, JSPS KAKENHI Grant Number 26430184 to HO, NASA Ocean Biology and Biogeochemistry program (NNX11AQ14G and NNX09AU43G) to EB, The Italian Research for the Sea (Flagship Project RITMARE) to DI, FWO, BIO5, Biosphere 2 to MBS. We also thank the support and commitment of Agnès b. and Etienne Bourgois, the Veolia Environment Foundation, Region Bretagne, Lorient Agglomeration, World Courier, Illumina, the EDF Foundation, FRB, the Prince Albert II de Monaco Foundation, the *Tara* schooner and its captains and crew. We thank MERCATOR-CORIOLIS and ACRI-ST for providing daily satellite data during the expedition. We are also grateful to the French Ministry of Foreign Affairs for supporting the expedition and to the countries who graciously granted sampling permissions. *Tara* Oceans would not exist without continuous support from 23 institutes (http://oceans.taraexpeditions.org). We also acknowledge excellent assistance from the European Bioinformatics Institute (EBI), in particular Guy Cochrane and Petra ten Hoopen, as well as the EMBL Advanced Light Microscopy Facility (ALMF), in particular Rainer Pepperkok. We thank Y. Timsit for stimulating scientific discussions and critical help during writing of the manuscript. The altimeter products were produced by Ssalto/Duacs and CLS with support from CNES. The authors further declare that all data reported herein are fully and freely available from the date of publication, with no

restrictions, and that all of the samples, analyses, publications, and ownership of data are free from legal entanglement or restriction of any sort by the various nations whose waters the *Tara* Oceans expedition sampled in. Data described herein is available at EBI and Pangaea (see Supplementary Table S1(44)), and the data release policy regarding future public release of *Tara* Oceans data is described in Pesant *et al* (44). All authors approved the final manuscript. This article is contribution number ZZZ of *Tara* Oceans.

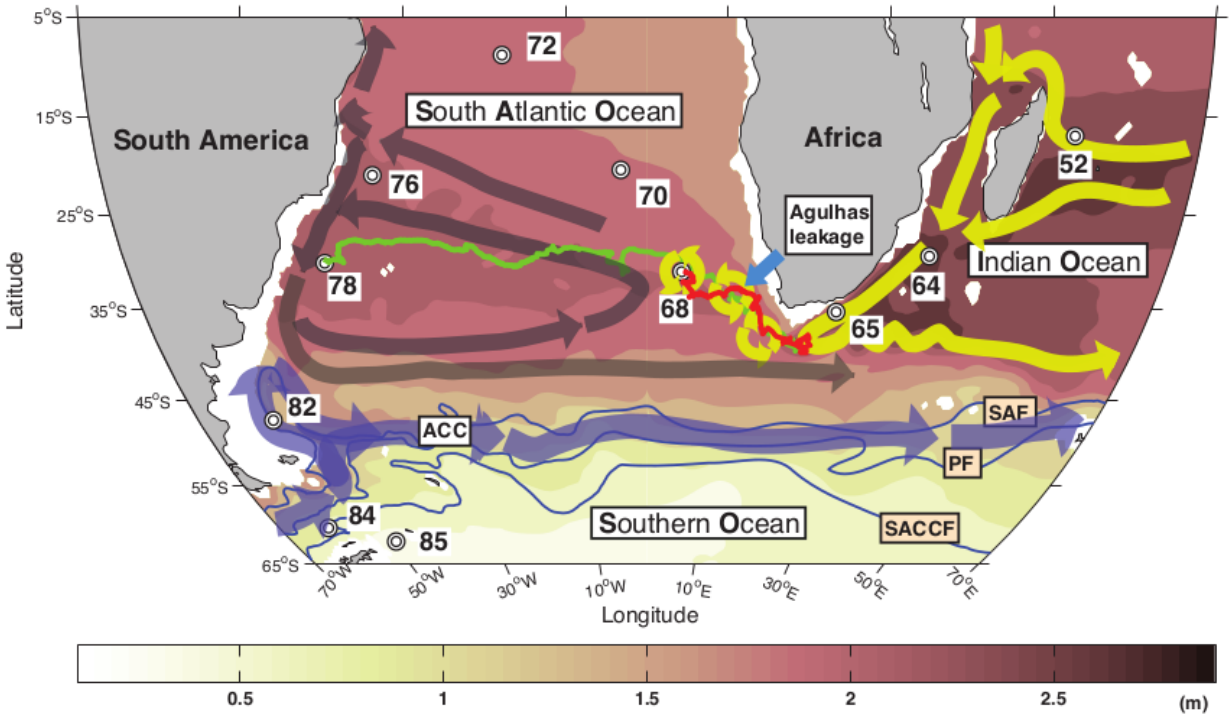

Fig. 1: The oceanic circulation around the Agulhas choke point and location of Tara Oceans stations.

The map shows the location of sampling stations, together with trajectories of the young and old Agulhas rings (TARA_68 & TARA_78, red and green tracks, respectively). The stations here considered as representative of the main basins are: 1) TARA_52, TARA_64, and TARA_65 for Indian Ocean (IO); 2) TARA_70, TARA_72 and TARA_76 for the South Atlantic Ocean (SAO) and 3) TARA_82, TARA_84 and TARA_85 for the Southern Ocean (SO). The mean ocean circulation is schematized by arrows (currents) and background colors (surface climatological dynamic height (0/2,000 dbar from CARS2009; www.cmar.csiro.au/cars, 61). Agulhas rings are depicted as circles. The ACC front positions are from (13).

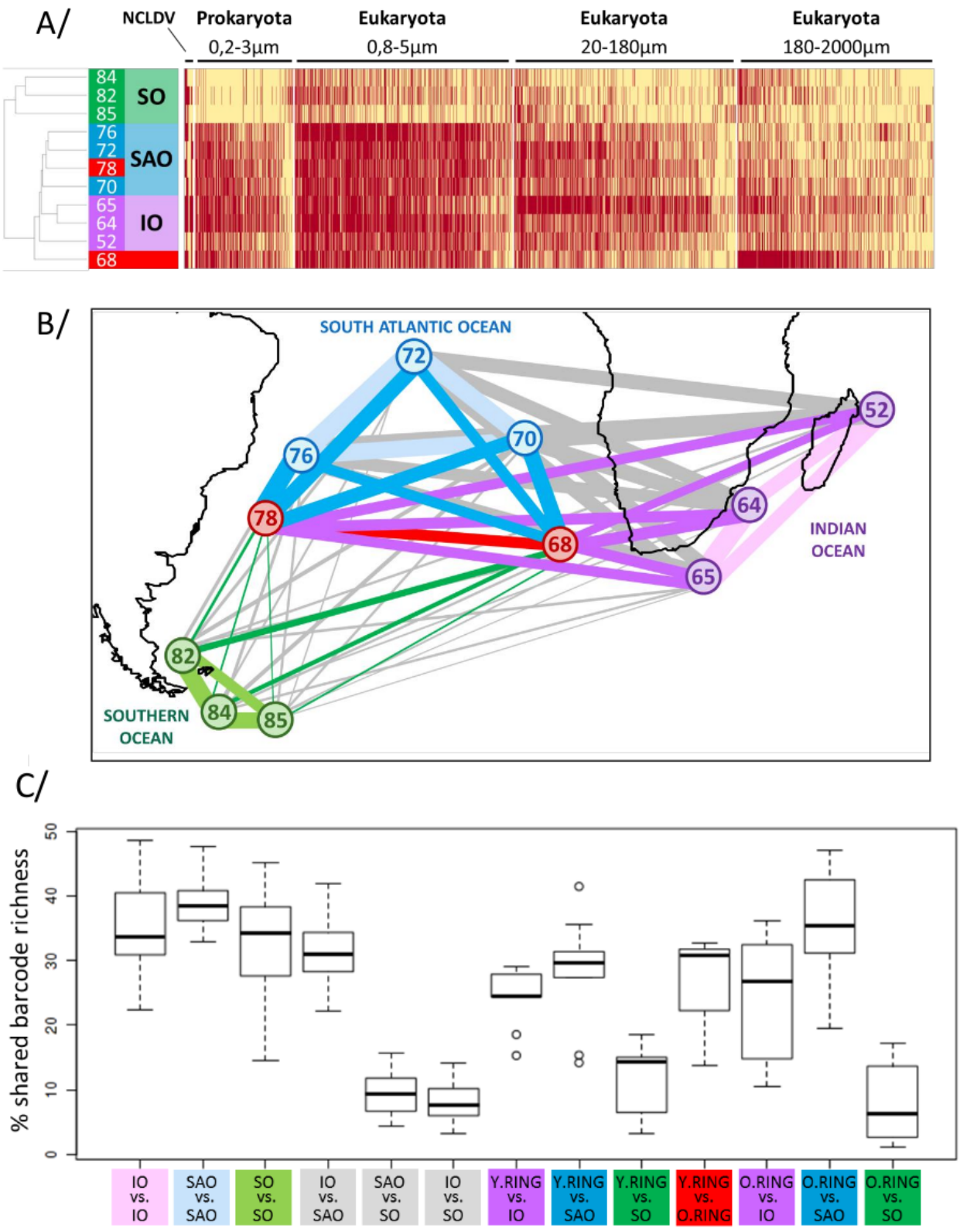

Fig. 2: Agulhas system plankton community structure

A/ Plankton community structure of the IO, SAO, SO and Agulhas rings. Bacterial 0.2-3 µm assemblage structure was determined by counting clade-specific marker-genes from bacterial metagenomes. Size fractionated (0.8-5, 20-180, 180-2 000 µm) eukaryotic assemblage structure was determined using V9 rDNA barcodes. Nucleo-Cytoplasmic Large DNA Viruses (NCLDV) 0.2-3 µm assemblage structure was determined by phylogenetic mapping using sixteen NCLDV marker genes. OTU abundances were converted to presence/absence to hierarchically cluster samples using Jaccard distance. B/ Network of pairwise comparisons of shared V9 rDNA barcode richness (shared barcode richness) between the 11 sampling stations of the study. The width of each edge is proportional to the number of shared barcodes between corresponding sampling stations. C/ Boxplot of shared barcode richness between stations for 0.8-5, 20-180 and 180-2 000 µm size fractions. The shared barcode richness analysis considers that two V9 rDNA barcodes are shared between two samples if they are 100% identical over their whole length. Shared barcode richness between two samples s1 & s2 is expressed as the proportion of shared barcode richness relative to the average internal barcode richness of samples s1 & s2. IO: Indian Ocean; SAO: South Atlantic Ocean, SO: Southern Ocean, Y.RING: Young Ring; O.RING: Old Ring.

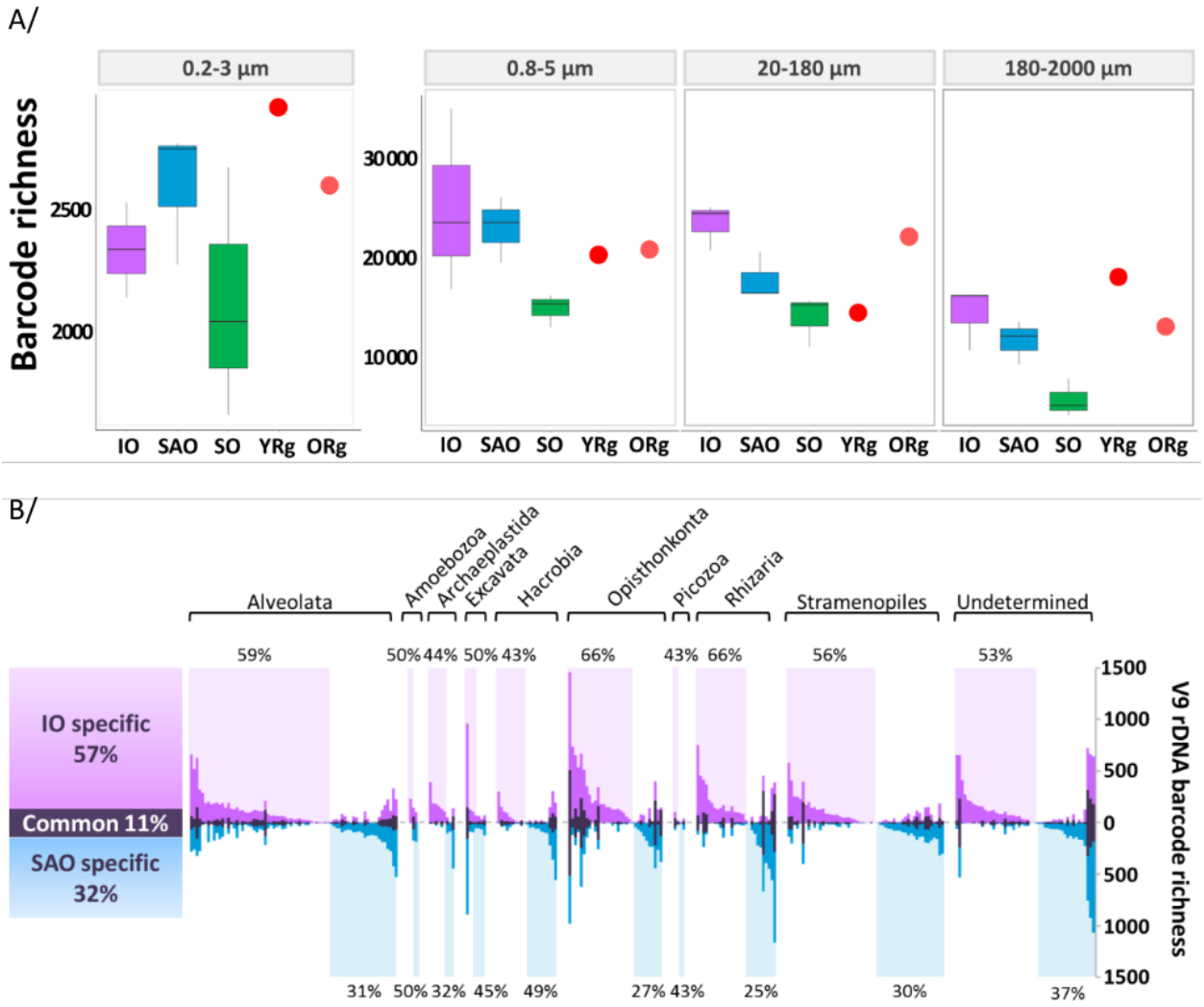

Fig. 3: Diversity of plankton population specific to Indian and Atlantic Oceans

A/ Boxplot of 16S (0.2-3 µm) and V9 rDNA barcodes richness (0.8-5, 20-180 and 180-2000 µm size fractions). Each box represents 3 sampling stations combined into IO, SAO and SO. Single Agulhas ring stations are represented as red (young ring) and orange (old ring) crosses. B/ Plankton sub-OTU richness filtering across the Agulhas choke point. Each vertical bar represents a single eukaryotic plankton OTU, each of which contains >10 distinct V9 rDNA barcodes (14). For each OTU are represented the number of distinct barcodes (sub-OTU richness) found exclusively in the SAO (blue), exclusively in the IO (pink), and in both SAO and IO (grey). OTUs are grouped by taxonomic annotation (indicated above the bar plot). For each taxonomic group, the percentage of OTUs with higher sub-OTU richness in the IO (shaded in pink) or in the SAO (shaded in blue) are indicated, respectively at the top and bottom of the bar plot. A total of 1307 OTUs are presented, representing 98% of total V9 rDNA barcode abundance.

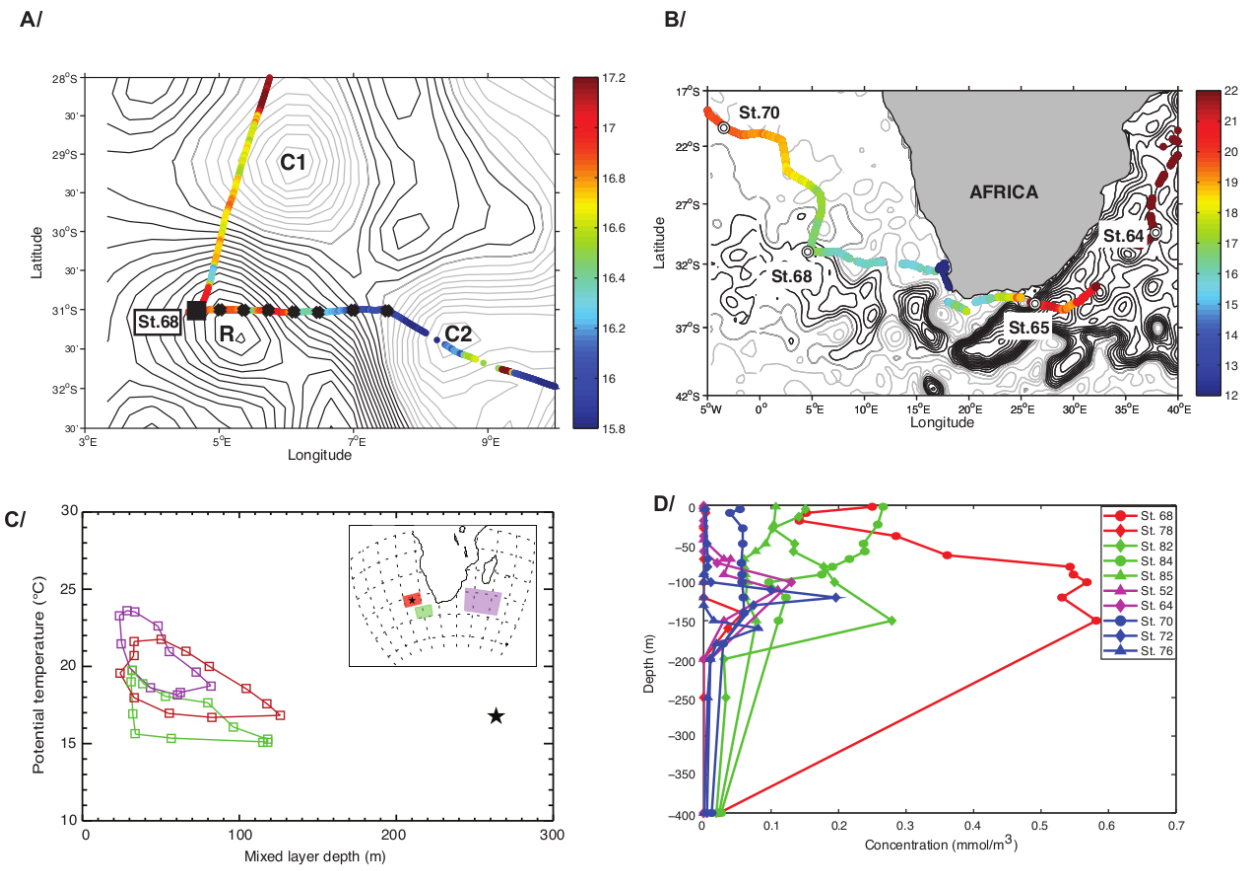

Fig. 4: Properties of the young Agulhas ring (TARA_68).
A/ Daily sea surface height around young Agulhas ring station TARA_68 (DT Absolute Dynamic Topography (ADT) from http://www.aviso.altimetry.fr/). R, C1 and C2 respectively denote the centers of the Agulhas ring and two cyclonic eddies. The contour interval is 0.02 dyn.m. The ADT values are for September 13th, 2010. Light grey isolines: ADT < 0.46 dyn. m. The crosses indicate the CTD stations while the square symbol indicates the position of the biological station TARA_68. The biological station coincides with the westernmost CTD station. ADT is affected by interpolation errors, which is why CTD casts were performed at sea to have a fine-scale description of the feature before defining the position of the biological station (23). Superimposed are the continuous underway temperatures (°C) from the on-board thermosalinograph. B/ Same as panel A but at the regional scale. Round symbols correspond to biological sampling stations. The contour interval is 0.1 dyn.m. C/ Seasonal distribution of the median values of the mixed layer depths and temperatures at 10m (from ARGO) provided by the IFREMER/LOS Mixed Layer Depth Climatology L2 database (www.ifremer.fr/cerweb/deboyer/mld) updated to July 27th 2011. The mixed layer is defined using a temperature criteria. The star symbol represents the young ring station TARA_68. Inset: geographic position of the areas used to select the mixed layer and temperature data. The mixed layer depth measured at TARA_68 is outside the 90th percentile of the distribution of mixed layer depths for the same month for both the subtropical (red and magenta) regions. The temperature matches the median for the same month and region of sampling. D/ Nitrites (NO_2) concentrations in mmol/m^3.

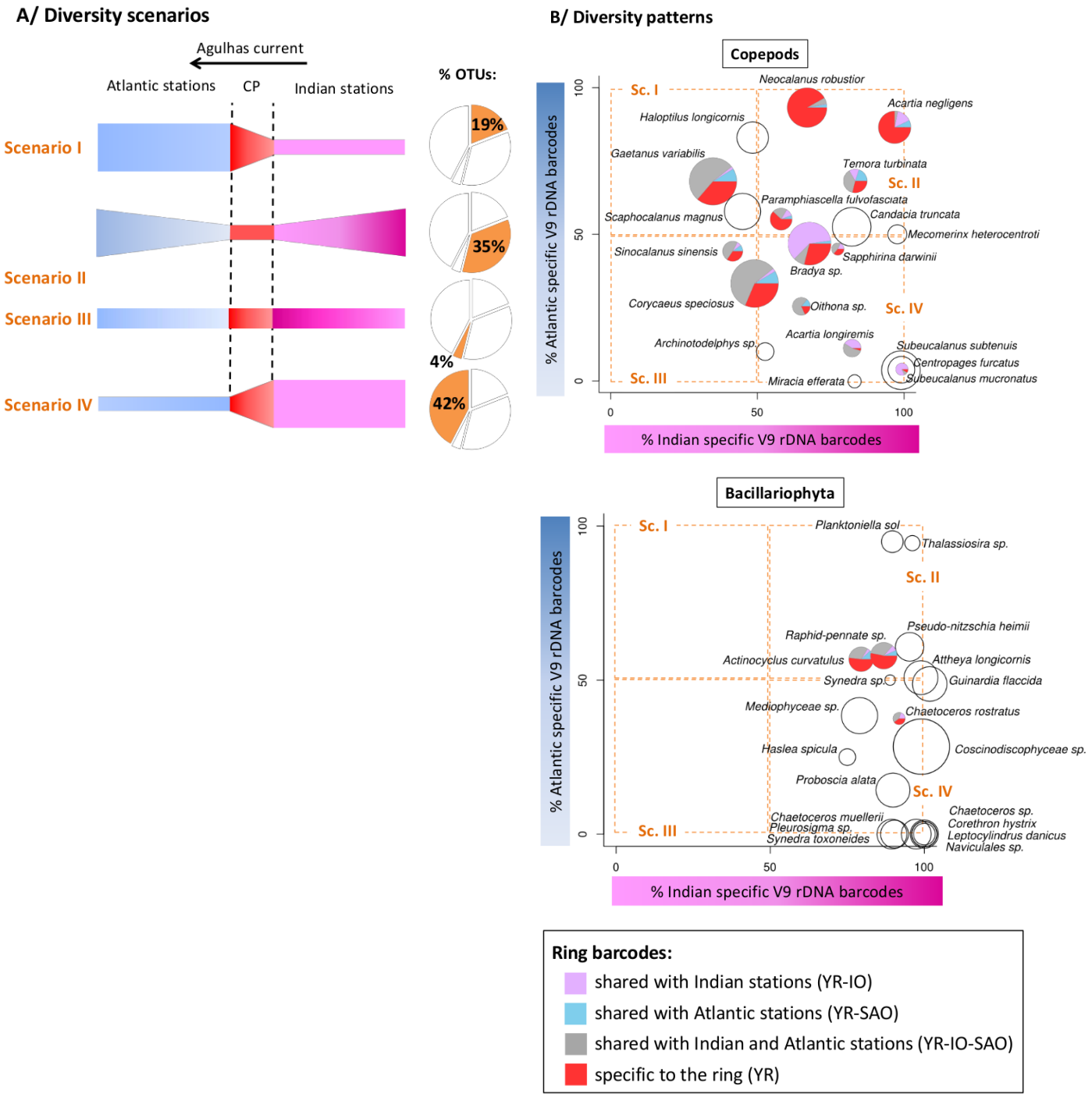

Fig. 5: Plankton diversity patterns.

A/ Schematic representation of the four scenarios (I-IV): plankton is transported from IO (pink, right) to SAO (blue, left) through the choke point (red, CP). The thickness of each colored section represents the level of diversity specific to each region. The observed percentage of V9 rDNA OTUs corresponding to each scenario is indicated in the pie charts to the left (out of 1063 OTUs of the full V9 rDNA barcode dataset). B/ V9 rDNA OTU diversity patterns for copepods and Bacillariophyta. Each circle on the charts represents a V9 rDNA OTU plotted with coordinates proportional to ribotypes specific to IO (x-axis) and SAO (y-axis). For instance, the

copepod *Acartia negligens* in the top right corner of sector II corresponds to the “bow tie” scenario II of panel A (*i.e.* a copepod with representative V9 rDNA barcodes in both IO and SAO, the vast majority of which are specific to their respective ocean basin). In contrast, the majority of barcodes for *Siloncalanus sinensis* in sector III are found in both IO and SAO (cosmopolitan OTU corresponding to the "Everything is everywhere" flat diversity diagram of panel A, scenario III). If more than 10 barcodes were found in the young Agulhas ring (TARA_68), their distribution is indicated in a pie chart (colors are coded in the legend inset), otherwise the OTU is represented by an empty circle. Circle sizes are proportional to the number of considered barcodes for each OTU. The Bacillariophyta OTU defined as ‘*Raphid pennate sp*.’ likely corresponds to the *Pseudo-nitzschia* cells observed by light microscopy.

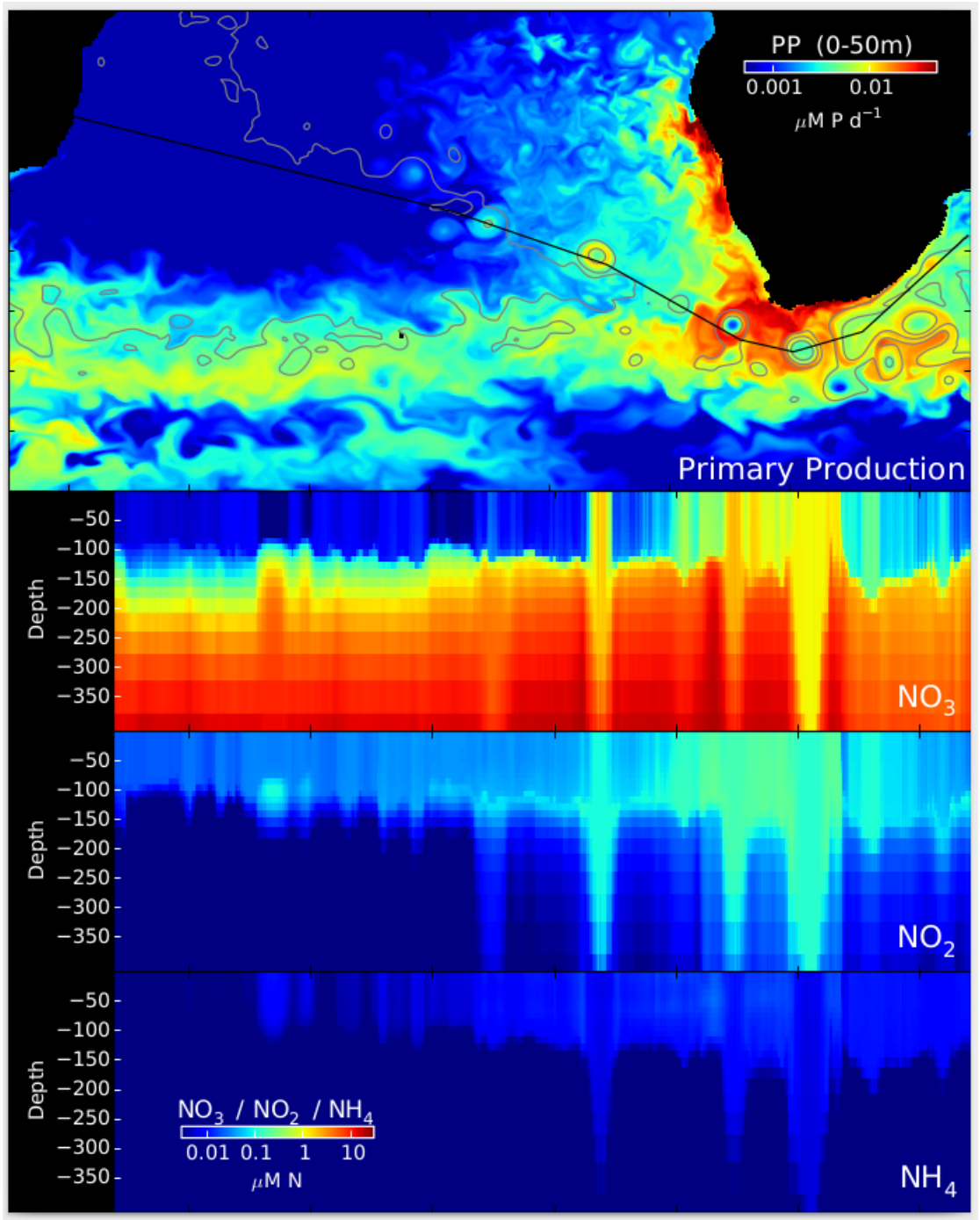

Fig. 6: Modeled nitrogen stocks along Agulhas ring track

A/ Simulated primary production (PP) in the Agulhas system using the MIT-GCM model. The solid black line shows the average northwesterly path of 12 distinct virtual Agulhas rings tracked over the course of the simulation. Color scale for PP is given in the top right inset, with warmer colors indicating higher PP. B/ Modeled profiles of NO_3, NO_2 and NH_4 along the Agulhas ring average track (x-axis) presented in A. The y-axis is the depth (in meters) in the water column. The color scale is given in the top right inset, with warmer colors indicating higher concentrations of nitrogen compounds.

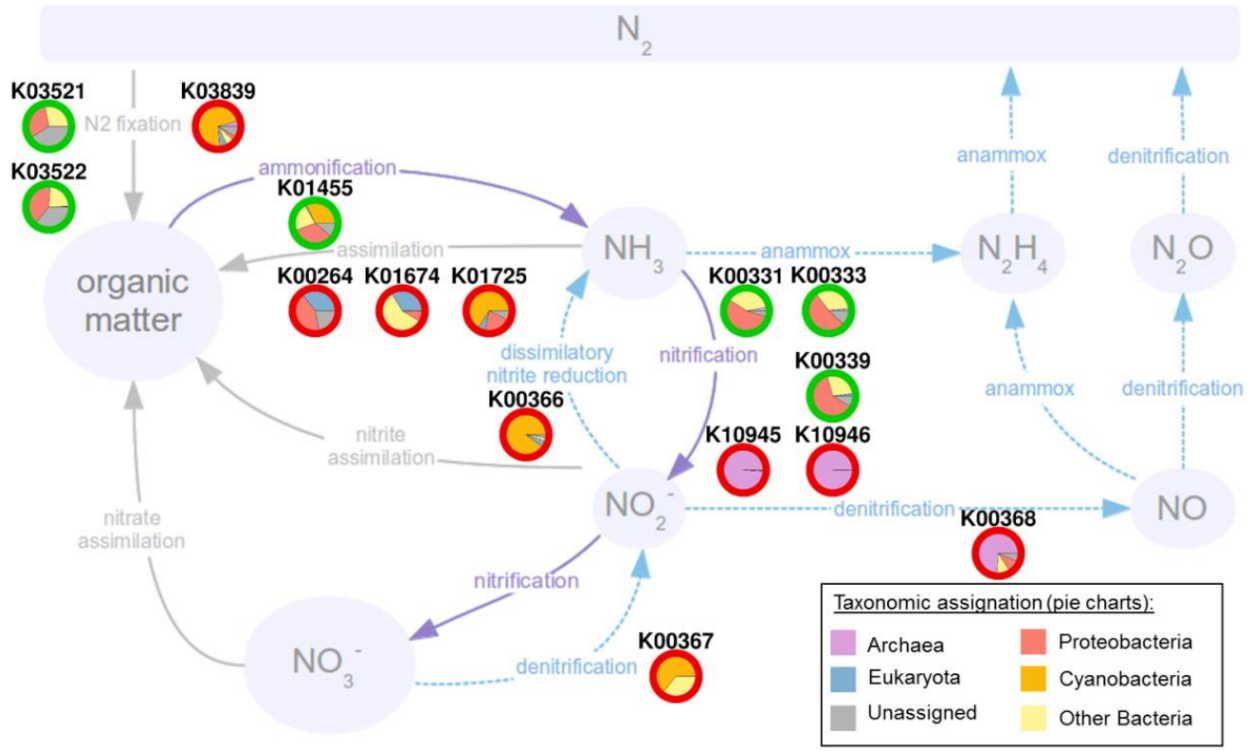

Fig. 7: Nitrite anomaly in young Agulhas ring is accompanied by shifts in nitrogen pathway related genes

Metagenomic over- and under-represented nitrogen pathway genes in young Agulhas ring. Over- (red circles) and under- (green circles) represented metagenome functional annotations (Kegg Orthologs, K#) involved in the nitrogen pathway in the young ring compared to IO and SAO reference stations, at surface and deep chlorophyll maximum depth. Pie charts inside circles represent the taxonomic distribution for each ortholog.

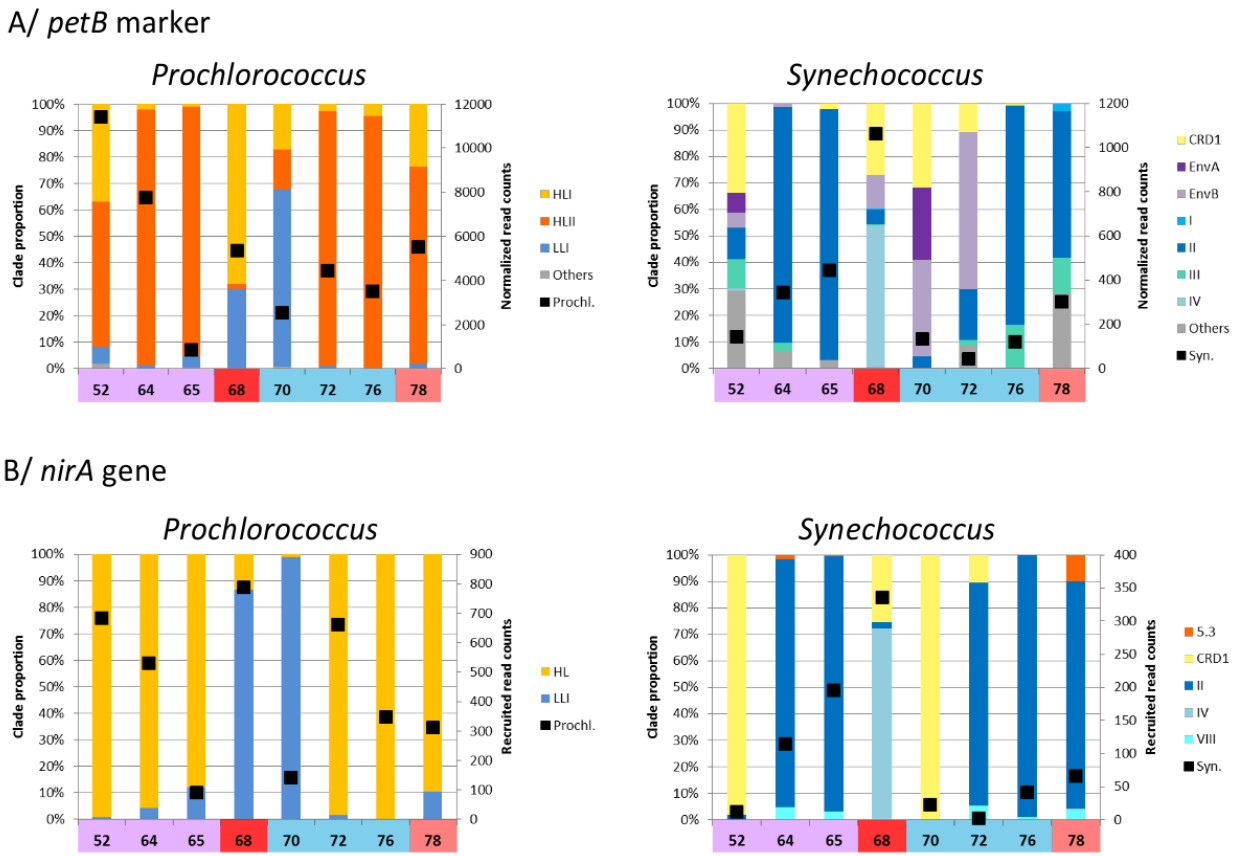

Fig. 8: Picocyanobacterial clade shift in the young Agulhas ring.

A/ Relative abundance of *Prochlorococcus* and *Synechococcus* clades estimated by *petB* read recruitments from 0.2-3 µm metagenomes. Solid squares correspond to read counts normalized based on the sequencing effort (right axis). B/ Relative abundance of *nirA* gene from *Prochlorococcus* and *Synechococcus* clades estimated by number of reads recruited from 0.2-3 µm metagenomes. The bar colors correspond to cyanobacterial clades indicated in the inset legends for each panel. Solid squares correspond to the number of reads recruited (right axis). Data is shown for stations 52 to 78 only as too few cyanobacteria were found in SO stations 82, 84 and 85.

Supplementary Materials:

Table S1, list of samples analysed.

Sample label [TARA_station#_environmental-feature_size-fraction]	PANGAEA sample identifier	Corresponding contextual data published at PANGAEA	Station identifier [TARA_station#]	Date/Time [yyyy-mm-ddThh:mm]	Latitude [degrees North]	Longitude [degrees East]	Sampling depth [m]
TARA_052_DCM_0.22-1.6	TARA_B100000214	http://www.pangaea.de/search?All&q=TARA_B100000214	TARA_052	2010-05-17T11:42	-16.9534	53.9601	75
TARA_052_SRF_0.22-1.6	TARA_B100000212	http://www.pangaea.de/search?All&q=TARA_B100000212	TARA_052	2010-05-17T04:10	-16.957	53.9801	5
TARA_052_SRF_0.8-5	TARA_N000000598	http://www.pangaea.de/search?All&q=TARA_N000000598	TARA_052	2010-05-17T04:10	-16.957	53.9801	5
TARA_052_SRF_20-180	TARA_N000000589	http://www.pangaea.de/search?All&q=TARA_N000000589	TARA_052	2010-05-17T06:48	-16.9672	53.9337	5
TARA_052_SRF_180-2000	TARA_N000000581	http://www.pangaea.de/search?All&q=TARA_N000000581	TARA_052	2010-05-17T04:10	-16.9567	53.9809	5
TARA_064_DCM_0.22-3	TARA_B100000405	http://www.pangaea.de/search?All&q=TARA_B100000405	TARA_064	2010-07-08T06:21	-29.5333	37.9117	65
TARA_064_SRF_0.22-3	TARA_B100000401	http://www.pangaea.de/search?All&q=TARA_B100000401	TARA_064	2010-07-07T04:48	-29.5019	37.9889	5
TARA_064_SRF_0.8-5	TARA_N000000522	http://www.pangaea.de/search?All&q=TARA_N000000522	TARA_064	2010-07-07T04:48	-29.5019	37.9889	5
TARA_064_SRF_20-180	TARA_N000000526	http://www.pangaea.de/search?All&q=TARA_N000000526	TARA_064	2010-07-07T07:53	-29.4985	37.9926	5
TARA_064_SRF_180-2000	TARA_N000000539	http://www.pangaea.de/search?All&q=TARA_N000000539	TARA_064	2010-07-07T05:17	-29.5018	37.9887	5
TARA_065_DCM_0.22-3	TARA_B000000441	http://www.pangaea.de/search?All&q=TARA_B000000441	TARA_065	2010-07-12T11:03:22	-35.2421	26.3048	30
TARA_065_SRF_0.22-3	TARA_B000000437	http://www.pangaea.de/search?All&q=TARA_B000000437	TARA_065	2010-07-12T05:59	-35.1728	26.2868	5
TARA_065_SRF_0.8-5	TARA_N000000959	http://www.pangaea.de/search?All&q=TARA_N000000959	TARA_065	2010-07-12T05:59	-35.1728	26.2868	5
TARA_065_SRF_20-180	TARA_N000000968	http://www.pangaea.de/search?All&q=TARA_N000000968	TARA_065	2010-07-12T10:30	-35.2351	26.3022	5
TARA_065_SRF_180-2000	TARA_N000000981	http://www.pangaea.de/search?All&q=TARA_N000000981	TARA_065	2010-07-12T06:36	-35.1808	26.2879	5
TARA_068_DCM_0.22-3	TARA_B100000482	http://www.pangaea.de/search?All&q=TARA_B100000482	TARA_068	2010-09-14T13:30	-31.027	4.6802	50
TARA_068_SRF_0.22-3	TARA_B100000475	http://www.pangaea.de/search?All&q=TARA_B100000475	TARA_068	2010-09-14T06:55	-31.0266	4.665	5
TARA_068_SRF_0.8-5	TARA_N000000722	http://www.pangaea.de/search?All&q=TARA_N000000722	TARA_068	2010-09-14T06:55	-31.0266	4.665	5
TARA_068_SRF_20-180	TARA_N000000705	http://www.pangaea.de/search?All&q=TARA_N000000705	TARA_068	2010-09-13T21:35	-31.0551	4.668	5
TARA_068_SRF_180-2000	TARA_N000000709	http://www.pangaea.de/search?All&q=TARA_N000000709	TARA_068	2010-09-13T20:20	-31.0507	4.6603	5
TARA_070_SRF_0.22-3	TARA_B100000459	http://www.pangaea.de/search?All&q=TARA_B100000459	TARA_070	2010-09-21T06:55	-20.4091	-3.1759	5
TARA_070_SRF_0.8-5	TARA_N000000678	http://www.pangaea.de/search?All&q=TARA_N000000678	TARA_070	2010-09-21T06:55	-20.4091	-3.1759	5
TARA_070_SRF_20-180	TARA_N000000662	http://www.pangaea.de/search?All&q=TARA_N000000662	TARA_070	2010-09-21T08:23	-20.3943	-3.2085	5
TARA_070_SRF_180-2000	TARA_N000000666	http://www.pangaea.de/search?All&q=TARA_N000000666	TARA_070	2010-09-21T07:22	-20.4035	-3.1859	5
TARA_072_DCM_0.22-3	TARA_B100000427	http://www.pangaea.de/search?All&q=TARA_B100000427	TARA_072	2010-10-05T15:35	-8.7296	-17.9604	100
TARA_072_SRF_0.22-3	TARA_B100000424	http://www.pangaea.de/search?All&q=TARA_B100000424	TARA_072	2010-10-05T08:00	-8.7789	-17.9099	5
TARA_072_SRF_0.8-5	TARA_N000000831	http://www.pangaea.de/search?All&q=TARA_N000000831	TARA_072	2010-10-05T08:00	-8.7789	-17.9099	5
TARA_072_SRF_20-180	TARA_N000000839	http://www.pangaea.de/search?All&q=TARA_N000000839	TARA_072	2010-10-05T09:48	-8.7484	-17.9179	5
TARA_072_SRF_180-2000	TARA_N000000843	http://www.pangaea.de/search?All&q=TARA_N000000843	TARA_072	2010-10-05T08:20	-8.7726	-17.915	5
TARA_076_DCM_0.22-3	TARA_B100000519	http://www.pangaea.de/search?All&q=TARA_B100000519	TARA_076	2010-10-16T16:58:37	-21.0292	-35.3498	150
TARA_076_SRF_0.22-3	TARA_B100000513	http://www.pangaea.de/search?All&q=TARA_B100000513	TARA_076	2010-10-16T09:55	-20.9354	-35.1803	5
TARA_076_SRF_0.8-5	TARA_N000000855	http://www.pangaea.de/search?All&q=TARA_N000000855	TARA_076	2010-10-16T09:55	-20.9354	-35.1803	5
TARA_076_SRF_20-180	TARA_N000000871	http://www.pangaea.de/search?All&q=TARA_N000000871	TARA_076	2010-10-16T11:18	-20.9514	-35.2273	5
TARA_076_SRF_180-2000	TARA_N000000879	http://www.pangaea.de/search?All&q=TARA_N000000879	TARA_076	2010-10-16T10:16	-20.9406	-35.196	5
TARA_078_DCM_0.22-3	TARA_B100000530	http://www.pangaea.de/search?All&q=TARA_B100000530	TARA_078	2010-11-04T18:16:53	-30.1484	-43.2705	120
TARA_078_SRF_0.22-3	TARA_B100000524	http://www.pangaea.de/search?All&q=TARA_B100000524	TARA_078	2010-11-04T10:04	-30.1367	-43.2899	5
TARA_078_SRF_0.8-5	TARA_N000000620	http://www.pangaea.de/search?All&q=TARA_N000000620	TARA_078	2010-11-04T10:04	-30.1367	-43.2899	5
TARA_078_SRF_20-180	TARA_N000001510	http://www.pangaea.de/search?All&q=TARA_N000001510	TARA_078	2010-11-04T13:22	-30.1872	-43.2834	5
TARA_078_SRF_180-2000	TARA_N000001514	http://www.pangaea.de/search?All&q=TARA_N000001514	TARA_078	2010-11-04T11:31	-30.1506	-43.2877	5
TARA_082_DCM_0.22-3	TARA_B100000767	http://www.pangaea.de/search?All&q=TARA_B100000767	TARA_082	2010-12-06T18:58	-47.2007	-57.9446	40
TARA_082_SRF_0.22-3	TARA_B100000768	http://www.pangaea.de/search?All&q=TARA_B100000768	TARA_082	2010-12-06T10:33	-47.1863	-58.2902	5
TARA_082_SRF_0.8-5	TARA_N000001386	http://www.pangaea.de/search?All&q=TARA_N000001386	TARA_082	2010-12-06T10:33	-47.1863	-58.2902	5
TARA_082_SRF_20-180	TARA_N000001394	http://www.pangaea.de/search?All&q=TARA_N000001394	TARA_082	2010-12-06T12:32	-47.1966	-58.2349	5
TARA_082_SRF_180-2000	TARA_N000001398	http://www.pangaea.de/search?All&q=TARA_N000001398	TARA_082	2010-12-06T11:34	-47.1899	-58.2724	5
TARA_084_SRF_0.22-3	TARA_B100000780	http://www.pangaea.de/search?All&q=TARA_B100000780	TARA_084	2011-01-03T11:05	-60.2287	-60.6476	5
TARA_084_SRF_0.8-5	TARA_N000001438	http://www.pangaea.de/search?All&q=TARA_N000001438	TARA_084	2011-01-03T11:05	-60.2287	-60.6476	5
TARA_084_SRF_20-180	TARA_N000001442	http://www.pangaea.de/search?All&q=TARA_N000001442	TARA_084	2011-01-03T13:58	-60.3046	-60.5715	5
TARA_084_SRF_180-2000	TARA_N000001362	http://www.pangaea.de/search?All&q=TARA_N000001362	TARA_084	2011-01-03T12:17	-60.2584	-60.6226	5
TARA_085_DCM_0.22-3	TARA_B100000795	http://www.pangaea.de/search?All&q=TARA_B100000795	TARA_085	2011-01-06T19:34:21	-62.2231	-49.2139	90
TARA_085_SRF_0.22-3	TARA_B100000787	http://www.pangaea.de/search?All&q=TARA_B100000787	TARA_085	2011-01-06T10:38	-62.0385	-49.529	5
TARA_085_SRF_0.8-5	TARA_N000001028	http://www.pangaea.de/search?All&q=TARA_N000001028	TARA_085	2011-01-06T10:38	-62.0385	-49.529	5
TARA_085_SRF_20-180	TARA_N000001036	http://www.pangaea.de/search?All&q=TARA_N000001036	TARA_085	2011-01-06T15:29	-62.14	-49.3273	5
TARA_085_SRF_180-2000	TARA_N000001040	http://www.pangaea.de/search?All&q=TARA_N000001040	TARA_085	2011-01-06T12:45	-62.0773	-49.4534	5

Environmental Feature	Size fraction lower threshold [micrometre]	Size fraction upper threshold [micrometre]	Marine pelagic biomes (Longhurst 2007)	Ocean and sea regions (IHO General Sea Areas 1953) [MRGID registered at www.marineregions.com]	Marine pelagic biomes (Longhurst 2007) [MRGID registered at www.marineregions.com]
(DCM) deep chlorophyll maximum layer (ENVO:01000326)	0.22	1.6	Trades Biome	(IO) Indian Ocean [MRGID:1904]	(ISSG) Indian South Subtropical Gyre Province [MRGID:21472]
(SRF) surface water layer (ENVO:00002042)	0.22	1.6	Trades Biome	(IO) Indian Ocean [MRGID:1904]	(ISSG) Indian South Subtropical Gyre Province [MRGID:21472]
(SRF) surface water layer (ENVO:00002042)	0.8	5	Trades Biome	(IO) Indian Ocean [MRGID:1904]	(ISSG) Indian South Subtropical Gyre Province [MRGID:21472]
(SRF) surface water layer (ENVO:00002042)	20	180	Trades Biome	(IO) Indian Ocean [MRGID:1904]	(ISSG) Indian South Subtropical Gyre Province [MRGID:21472]
(SRF) surface water layer (ENVO:00002042)	180	2000	Trades Biome	(IO) Indian Ocean [MRGID:1904]	(ISSG) Indian South Subtropical Gyre Province [MRGID:21472]
(DCM) deep chlorophyll maximum layer (ENVO:01000326)	0.22	3	Coastal Biome	(IO) Indian Ocean [MRGID:1904]	(EAFR) Eastern Africa Coastal Province [MRGID:21473]
(SRF) surface water layer (ENVO:00002042)	0.22	3	Coastal Biome	(IO) Indian Ocean [MRGID:1904]	(EAFR) Eastern Africa Coastal Province [MRGID:21473]
(SRF) surface water layer (ENVO:00002042)	0.8	5	Coastal Biome	(IO) Indian Ocean [MRGID:1904]	(EAFR) Eastern Africa Coastal Province [MRGID:21473]
(SRF) surface water layer (ENVO:00002042)	20	180	Coastal Biome	(IO) Indian Ocean [MRGID:1904]	(EAFR) Eastern Africa Coastal Province [MRGID:21473]
(SRF) surface water layer (ENVO:00002042)	180	2000	Coastal Biome	(IO) Indian Ocean [MRGID:1904]	(EAFR) Eastern Africa Coastal Province [MRGID:21473]
(DCM) deep chlorophyll maximum layer (ENVO:01000326)	0.22	3	Coastal Biome	(IO) Indian Ocean [MRGID:1904]	(EAFR) Eastern Africa Coastal Province [MRGID:21473]
(SRF) surface water layer (ENVO:00002042)	0.22	3	Coastal Biome	(IO) Indian Ocean [MRGID:1904]	(EAFR) Eastern Africa Coastal Province [MRGID:21473]
(SRF) surface water layer (ENVO:00002042)	0.8	5	Coastal Biome	(IO) Indian Ocean [MRGID:1904]	(EAFR) Eastern Africa Coastal Province [MRGID:21473]
(SRF) surface water layer (ENVO:00002042)	20	180	Coastal Biome	(IO) Indian Ocean [MRGID:1904]	(EAFR) Eastern Africa Coastal Province [MRGID:21473]
(SRF) surface water layer (ENVO:00002042)	180	2000	Coastal Biome	(IO) Indian Ocean [MRGID:1904]	(EAFR) Eastern Africa Coastal Province [MRGID:21473]
(DCM) deep chlorophyll maximum layer (ENVO:01000326)	0.22	3	Trades Biome	(SAO) South Atlantic Ocean [MRGID:1914]	(SATL) South Atlantic Gyral Province [MRGID:21459]
(SRF) surface water layer (ENVO:00002042)	0.22	3	Trades Biome	(SAO) South Atlantic Ocean [MRGID:1914]	(SATL) South Atlantic Gyral Province [MRGID:21459]
(SRF) surface water layer (ENVO:00002042)	0.8	5	Trades Biome	(SAO) South Atlantic Ocean [MRGID:1914]	(SATL) South Atlantic Gyral Province [MRGID:21459]
(SRF) surface water layer (ENVO:00002042)	20	180	Trades Biome	(SAO) South Atlantic Ocean [MRGID:1914]	(SATL) South Atlantic Gyral Province [MRGID:21459]
(SRF) surface water layer (ENVO:00002042)	180	2000	Trades Biome	(SAO) South Atlantic Ocean [MRGID:1914]	(SATL) South Atlantic Gyral Province [MRGID:21459]
(SRF) surface water layer (ENVO:00002042)	0.22	3	Trades Biome	(SAO) South Atlantic Ocean [MRGID:1914]	(SATL) South Atlantic Gyral Province [MRGID:21459]
(SRF) surface water layer (ENVO:00002042)	0.8	5	Trades Biome	(SAO) South Atlantic Ocean [MRGID:1914]	(SATL) South Atlantic Gyral Province [MRGID:21459]
(SRF) surface water layer (ENVO:00002042)	20	180	Trades Biome	(SAO) South Atlantic Ocean [MRGID:1914]	(SATL) South Atlantic Gyral Province [MRGID:21459]
(SRF) surface water layer (ENVO:00002042)	180	2000	Trades Biome	(SAO) South Atlantic Ocean [MRGID:1914]	(SATL) South Atlantic Gyral Province [MRGID:21459]
(DCM) deep chlorophyll maximum layer (ENVO:01000326)	0.22	3	Trades Biome	(SAO) South Atlantic Ocean [MRGID:1914]	(SATL) South Atlantic Gyral Province [MRGID:21459]
(SRF) surface water layer (ENVO:00002042)	0.22	3	Trades Biome	(SAO) South Atlantic Ocean [MRGID:1914]	(SATL) South Atlantic Gyral Province [MRGID:21459]
(SRF) surface water layer (ENVO:00002042)	0.8	5	Trades Biome	(SAO) South Atlantic Ocean [MRGID:1914]	(SATL) South Atlantic Gyral Province [MRGID:21459]
(SRF) surface water layer (ENVO:00002042)	20	180	Trades Biome	(SAO) South Atlantic Ocean [MRGID:1914]	(SATL) South Atlantic Gyral Province [MRGID:21459]
(SRF) surface water layer (ENVO:00002042)	180	2000	Trades Biome	(SAO) South Atlantic Ocean [MRGID:1914]	(SATL) South Atlantic Gyral Province [MRGID:21459]
(DCM) deep chlorophyll maximum layer (ENVO:01000326)	0.22	3	Trades Biome	(SAO) South Atlantic Ocean [MRGID:1914]	(SATL) South Atlantic Gyral Province [MRGID:21459]
(SRF) surface water layer (ENVO:00002042)	0.22	3	Trades Biome	(SAO) South Atlantic Ocean [MRGID:1914]	(SATL) South Atlantic Gyral Province [MRGID:21459]
(SRF) surface water layer (ENVO:00002042)	0.8	5	Trades Biome	(SAO) South Atlantic Ocean [MRGID:1914]	(SATL) South Atlantic Gyral Province [MRGID:21459]
(SRF) surface water layer (ENVO:00002042)	20	180	Trades Biome	(SAO) South Atlantic Ocean [MRGID:1914]	(SATL) South Atlantic Gyral Province [MRGID:21459]
(SRF) surface water layer (ENVO:00002042)	180	2000	Trades Biome	(SAO) South Atlantic Ocean [MRGID:1914]	(SATL) South Atlantic Gyral Province [MRGID:21459]
(DCM) deep chlorophyll maximum layer (ENVO:01000326)	0.22	3	Trades Biome	(SAO) South Atlantic Ocean [MRGID:1914]	(SATL) South Atlantic Gyral Province [MRGID:21459]
(SRF) surface water layer (ENVO:00002042)	0.22	3	Trades Biome	(SAO) South Atlantic Ocean [MRGID:1914]	(SATL) South Atlantic Gyral Province [MRGID:21459]
(SRF) surface water layer (ENVO:00002042)	0.8	5	Trades Biome	(SAO) South Atlantic Ocean [MRGID:1914]	(SATL) South Atlantic Gyral Province [MRGID:21459]
(SRF) surface water layer (ENVO:00002042)	20	180	Trades Biome	(SAO) South Atlantic Ocean [MRGID:1914]	(SATL) South Atlantic Gyral Province [MRGID:21459]
(SRF) surface water layer (ENVO:00002042)	180	2000	Trades Biome	(SAO) South Atlantic Ocean [MRGID:1914]	(SATL) South Atlantic Gyral Province [MRGID:21459]
(DCM) deep chlorophyll maximum layer (ENVO:01000326)	0.22	3	Coastal Biome	(SAO) South Atlantic Ocean [MRGID:1914]	(FKLD) Southwest Atlantic Shelves Province [MRGID:21469]
(SRF) surface water layer (ENVO:00002042)	0.22	3	Coastal Biome	(SAO) South Atlantic Ocean [MRGID:1914]	(FKLD) Southwest Atlantic Shelves Province [MRGID:21469]
(SRF) surface water layer (ENVO:00002042)	0.8	5	Coastal Biome	(SAO) South Atlantic Ocean [MRGID:1914]	(FKLD) Southwest Atlantic Shelves Province [MRGID:21469]
(SRF) surface water layer (ENVO:00002042)	20	180	Coastal Biome	(SAO) South Atlantic Ocean [MRGID:1914]	(FKLD) Southwest Atlantic Shelves Province [MRGID:21469]
(SRF) surface water layer (ENVO:00002042)	180	2000	Coastal Biome	(SAO) South Atlantic Ocean [MRGID:1914]	(FKLD) Southwest Atlantic Shelves Province [MRGID:21469]
(SRF) surface water layer (ENVO:00002042)	0.22	3	Polar Biome	(SO) Southern Ocean [MRGID:1907]	(ANTA) Antarctic Province [MRGID:21502]
(SRF) surface water layer (ENVO:00002042)	0.8	5	Polar Biome	(SO) Southern Ocean [MRGID:1907]	(ANTA) Antarctic Province [MRGID:21502]
(SRF) surface water layer (ENVO:00002042)	20	180	Polar Biome	(SO) Southern Ocean [MRGID:1907]	(ANTA) Antarctic Province [MRGID:21502]
(SRF) surface water layer (ENVO:00002042)	180	2000	Polar Biome	(SO) Southern Ocean [MRGID:1907]	(ANTA) Antarctic Province [MRGID:21502]
(DCM) deep chlorophyll maximum layer (ENVO:01000326)	0.22	3	Polar Biome	(SO) Southern Ocean [MRGID:1907]	(ANTA) Antarctic Province [MRGID:21502]
(SRF) surface water layer (ENVO:00002042)	0.22	3	Polar Biome	(SO) Southern Ocean [MRGID:1907]	(ANTA) Antarctic Province [MRGID:21502]
(SRF) surface water layer (ENVO:00002042)	0.8	5	Polar Biome	(SO) Southern Ocean [MRGID:1907]	(ANTA) Antarctic Province [MRGID:21502]
(SRF) surface water layer (ENVO:00002042)	20	180	Polar Biome	(SO) Southern Ocean [MRGID:1907]	(ANTA) Antarctic Province [MRGID:21502]
(SRF) surface water layer (ENVO:00002042)	180	2000	Polar Biome	(SO) Southern Ocean [MRGID:1907]	(ANTA) Antarctic Province [MRGID:21502]